

Different polyaniline/carbon nanotube composites as Pt catalyst supports for methanol electro-oxidation

Xingwei Li · Jiadi Wei · Yuzheng Chai ·
Shuo Zhang · Min Zhou

Received: 20 August 2014 / Accepted: 14 October 2014 / Published online: 21 October 2014
© Springer Science+Business Media New York 2014

Abstract Polyaniline/carbon nanotube composites as Pt catalyst supports for methanol electro-oxidation have been reported. Conventionally, the size and distribution of Pt catalysts were improved in the presence of polyaniline (PAni), and an interaction between Pt and N atoms in PAni could prevent Pt catalysts from aggregation and detachment. In this work, polyaniline-modified multi-walled carbon nanotube (PAni-MWCNT) composites, with different loading levels of PAni, were synthesized by in situ oxidative polymerization of aniline on the surface of MWCNT. And Pt catalysts supported by these composites were prepared by the liquid phase reduction. Our studies revealed that the loading level of PAni affected the proportion of the different valence Pt components. And the proportion of Pt(0) and Pt(II) was also important for improving the electro-catalytic performance of Pt catalysts. The proper proportion of Pt(II) was essential for coordination of Pt with oxygen-containing ligands (OH, H₂O) and thus accelerating oxidation of Pt (CO)_{ads} with release of CO₂ by improving the tolerance to intermediate carbonaceous species.

Introduction

In the past few years, the world's ever increasing energy demands, continuous and rapid consumption of fossil fuels and the global climate change due to the combustion of fossil fuels have sparked people around the world to seek a clean, sustainable, and greener energy source [1, 2]. Fuel cells are receiving widespread attention as an alternative to conventional fuel combustion power generation due to its high efficiency and environmental friendliness [3]. Among various types of fuel cells, direct methanol fuel cells (DMFCs) have been attracting enormous interests as portable power sources because of their simple design, high energy density, low operating temperature, and convenient fuel storage and supply [4, 5]. However, the production of low-cost catalysts with satisfactory catalytic performance and long-term durability still impedes their commercialization on large scale [5–7].

Pt-based catalysts are commonly used for DMFCs. For supported metal catalysts, such as metal particle size, size distribution, morphology, dispersion and stability, are strongly dependent on the nature of catalyst support, i.e., chemical compositions, specific surface area, porosity, electrical conductivity, electrochemical stability, and surface functional groups. Thus, in order to improve the performance of catalysts, an effective strategy is to develop novel supports to achieve high dispersion, efficiency, activity, and stability for catalysts [1, 4, 5]. An ideal support should meet the following criteria: (i) large specific surface area, (ii) moderate porosity, (iii) satisfactory electrical conductivity, (iv) favorable catalyst–support interaction, and (v) long-term durability [1, 8].

Unique properties of carbon materials make them the best candidate for electro-catalyst support [9, 10]. One of the most widely used carbon materials is carbon nanotube

X. Li (✉) · J. Wei · Y. Chai · M. Zhou
Shanghai Key Laboratory of Advanced Polymeric Materials,
Key Laboratory for Ultrafine Materials of Ministry of Education,
School of Materials Science and Engineering, East China
University of Science and Technology, Mei Long Road 130,
Shanghai 200237, People's Republic of China
e-mail: lixingwei_nj@yahoo.com; lixw_nj@126.com

S. Zhang
Department of Polymer Science, College of Polymer Science
and Polymer Engineering, The University of Akron, Akron,
OH 44325-3909, USA

(CNT) [11–13]. However, the surface of CNT is highly chemically inert due to high graphitization, and thus it is very difficult to deposit Pt particles directly and evenly onto such surface without functional groups. Moreover, Pt particles suffer from detachment from a support due to the low affinity between Pt and carbon atoms. Therefore, it is rather significantly challenging to deposit Pt catalysts onto the surface of CNT with reinforced binding strength between Pt and CNT [6]. In order to obtain high-performance Pt catalyst supported on CNT, CNT are often pre-treated with harsh oxidative procedures prior to use, such as refluxing in the concentrated mixture of HNO₃ and H₂SO₄. However, in that case, the graphitized surface of CNT is readily destroyed by erosion upon these procedures, which reduces the conductivity and durability of CNT.

A great deal of interest has been focused on conductive polymers due to their low resistance, good environmental stability, and easy synthesis [14, 15]. However, the degradation of conductive polymers is observed during both metal deposition and catalytic processes when used as catalyst supports [16]. Fortunately, with further researches, it has been found that the combination of conductive polymers and carbon materials offers an alternative toward composite supports, which are attractive for potential applications. In comparison to other conductive polymers, PANi is easy to synthesize, inexpensive, and Pt particles can strongly adhere to the surface of PANi due to an interaction between Pt and N atoms in PANi [6, 8]. The presence of PANi contributed to firm adhesion between Pt particles and supports and prevented Pt catalysts from aggregation and detachment [17]. However, to our best knowledge, other important factors affecting the performance of Pt catalysts have not fully studied for methanol electro-oxidation, except the size and distribution of Pt catalysts.

In this work, different PANi-MWCNT composites were prepared. And the performance of Pt catalysts, supported by these composites, was characterized via cyclic voltammograms (CV) and chronoamperometry (CA). Our work reveals that the loading level of PANi not only affects the size and distribution of Pt catalysts, but also influences the proportion of the different valence Pt components.

Experimental section

Materials

MWCNT (purity >95 %, diameter 10–20 nm, length ~30 μm) were provided by Chengdu Organic Chemicals Co. Ltd., Chinese Academy of Sciences. Aniline was obtained from Shanghai Lingfeng Reagent Co. Ltd. and

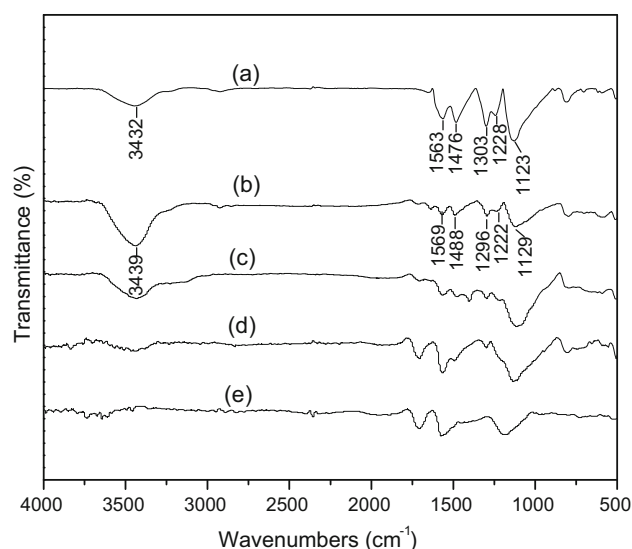


Fig. 1 FTIR spectra of PANi (a), PANi-MWCNT_{1:1} (b), PANi-MWCNT_{1:3} (c), PANi-MWCNT_{1:6} (d) and MWCNT (e)

purified via distillation under high-purity nitrogen. H₂PtCl₆ and NaBH₄ were purchased from Sigma-Aldrich and were used as received. All other chemicals were of analytical grade.

Preparation of PANi-MWCNT composites

PANi-MWCNT composites with feed molar ratios of 1:1, 1:3, and 1:6 (aniline: MWCNT) were prepared by the following strategy. 0.465 g MWCNT were dispersed in 50 mL 1.5 M HClO₄ under magnetic stirring to form a stable suspension, followed by addition of varied fractions of aniline and 25 mL 1.5 M HClO₄. Calculated amount of (NH₄)₂S₂O₈ (dissolved in 25 mL 1.5 M HClO₄) was added dropwise to the above suspension, and the suspension was stirred for 24 h at room temperature, yielding black precipitates of PANi-MWCNT composites with the different loading levels of PANi, labeled as PANi-MWCNT_{1:1}, PANi-MWCNT_{1:3}, and PANi-MWCNT_{1:6}, respectively. Black powder was obtained after the precipitates were washed copiously with de-ionized and collected with Buchner funnel.

Preparation of Pt/PANi-MWCNT catalysts

Pt/PANi-MWCNT catalysts were prepared by in situ liquid phase reduction using H₂PtCl₆ as a precursor. In typical procedures, 60 mg PANi-MWCNT was ultrasonicated in ethylene glycol/de-ionized water solution with volume ratio of 1:1 for 20 min, followed by the addition of 2 mL 0.0386 M H₂PtCl₆. The suspension was ultrasonicated

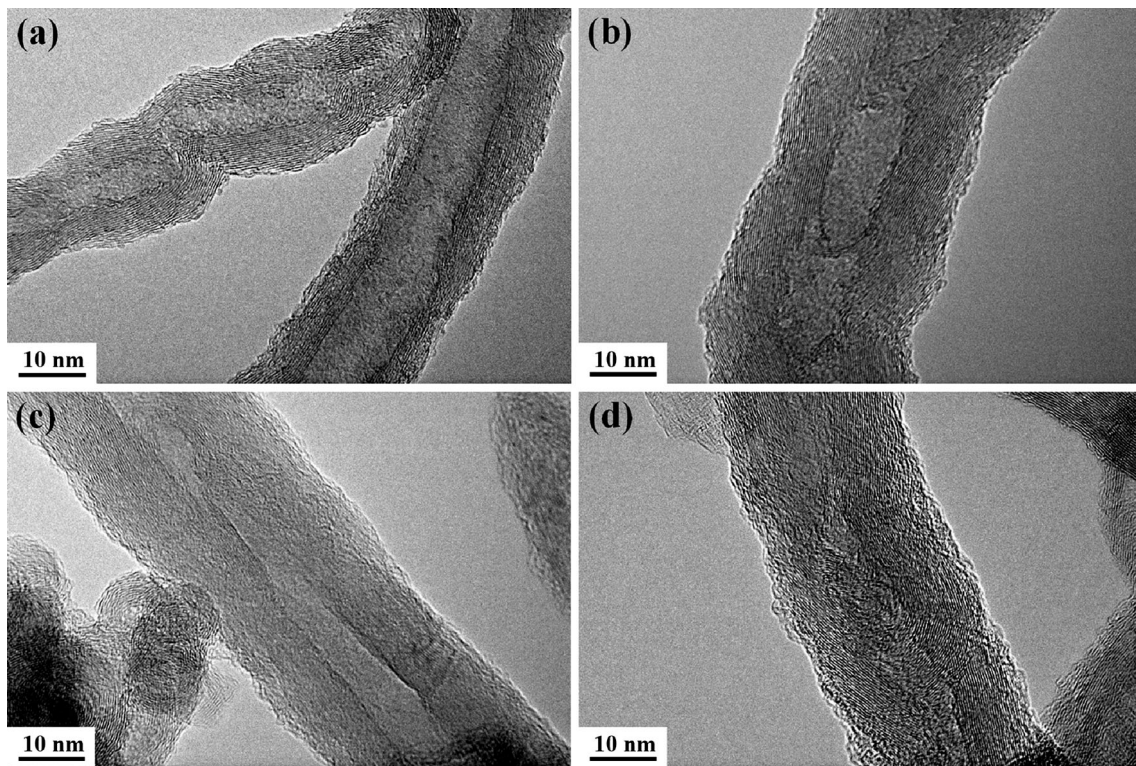


Fig. 2 TEM of MWCNT (a), PANi-MWCNT_{1:6} (b), PANi-MWCNT_{1:3} (c), PANi-MWCNT_{1:1} (d)

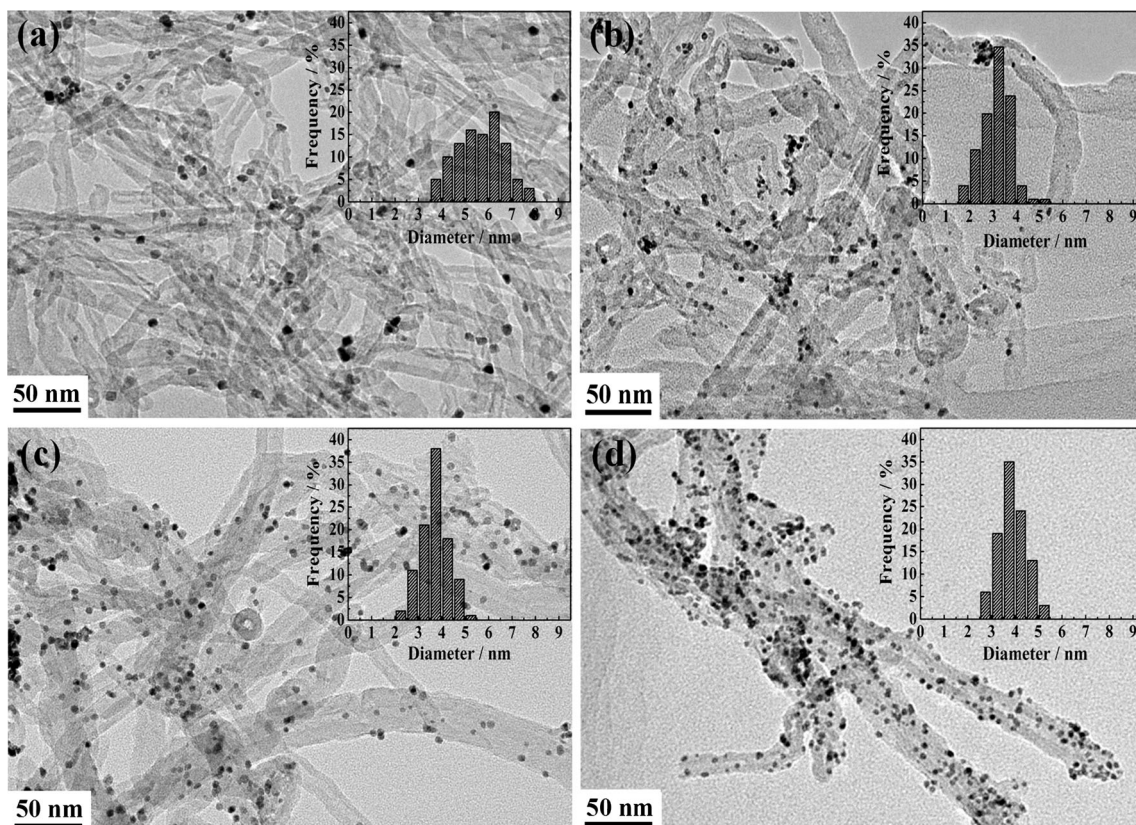


Fig. 3 TEM of Pt/MWCNT (a), Pt/PANi-MWCNT_{1:6} (b), Pt/PANi-MWCNT_{1:3} (c), Pt/PANi-MWCNT_{1:1} (d)

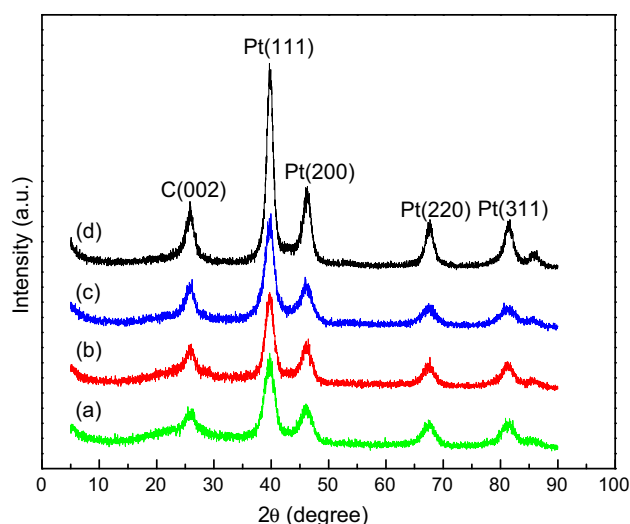


Fig. 4 XRD of Pt/PANI-MWCNT_{1:1} (a), Pt/PANI-MWCNT_{1:3} (b), Pt/PANI-MWCNT_{1:6} (c), Pt/MWCNT (d)

vigorously for additional 30 min at room temperature before 30 mg NaBH₄ powder was added, and the suspension was magnetically stirred for 2 h at 50–55 °C. The pH value of the reduction reaction was 8. The resulting slurry was filtered, washed thoroughly with de-ionized water, and dried at ambient conditions for 48 h, yielding black powder. Pt catalysts supported by different PANi-MWCNT composites were labeled as Pt/PANI-MWCNT_{1:1}, Pt/PANI-MWCNT_{1:3}, and Pt/PANI-MWCNT_{1:6}, respectively. Pt/MWCNT catalyst was also prepared in the absence of PANi via the same strategy for control purpose.

Characterization of structure and morphology

Fourier-transform infrared spectra (FTIR) of the powder sample were recorded on a Nicolet Magna-IR550 spectrometer. X-ray diffraction (XRD) was carried out with D/max2550VB/PC (Rigaku Co., Japan), using Cu K_α radiation ($\lambda = 1.54056 \text{ \AA}$), at operating voltage of 40 kV and current of 100 mA. The morphology was probed by a JEOL JEM-2010 transmission electron microscope (TEM). And the statistical average dimension of Pt catalyst was estimated from bright-field TEM images. X-ray photoelectron spectroscopy (XPS) was performed on an ESCA-LAB 250Xi spectrometer (Thermo Scientific) with Al K_α X-ray source for excitation. The binding energy (BE) was calibrated using a C 1s photoelectron peak at 284.6 eV as reference.

Electrochemical measurements

Electrochemical measurements were performed with a CHI 660C electrochemical analyzer in a standard three-

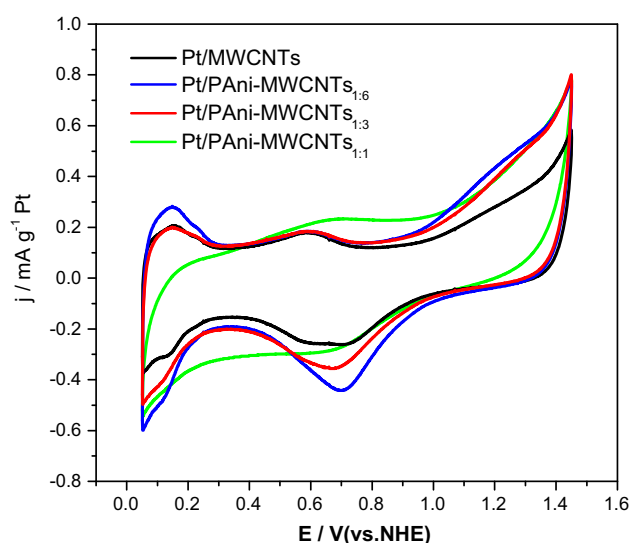


Fig. 5 CVs of the as-prepared catalysts in 0.5 M H₂SO₄ with the scan rate of 50 mV s⁻¹

electrode electrochemical cell. The working electrode was a glassy carbon (GC) electrode with diameter of 3 mm. A Pt wire electrode and a saturated calomel reference electrode (SCE) were used as the counter and reference electrode, respectively, but all the potentials in this study were reported versus normal hydrogen electrode (NHE). The working electrode was prepared via the following procedures. 2 mg of catalyst was added to 1 mL de-ionized water and ultrasonicated for a few minutes to obtain a homogeneous suspension solution (2 mg mL⁻¹). 10 μ L of the above suspension was drop-cast onto a freshly polished GC electrode. After dried, 5 μ L of Nafion solution (5 wt%) was sequentially drop-cast onto the surface of the catalyst electrode. After the solvent evaporated, the working electrodes were obtained.

The catalytic performance was studied by cyclic voltammograms (CV) and chronoamperometry (CA). CV curves were recorded in 0.5 M CH₃OH and 0.5 M H₂SO₄ solution with a scan rate of 50 mV s⁻¹. CA curves were obtained by polarization at a fixed potential of 0.75 V (vs. NHE) for 1000 s. High-purity nitrogen was purged for 15 min before measurement.

Results and discussion

FTIR spectra and morphology of PANi-MWCNT composites

FTIR spectra of PANi, PANi-MWCNT_{1:1}, PANi-MWCNT_{1:3}, PANi-MWCNT_{1:6} and MWCNT were shown in Fig. 1.

For PANi, the absorption band at 3432 cm⁻¹ was attributable to N–H stretching vibration, and the bands at

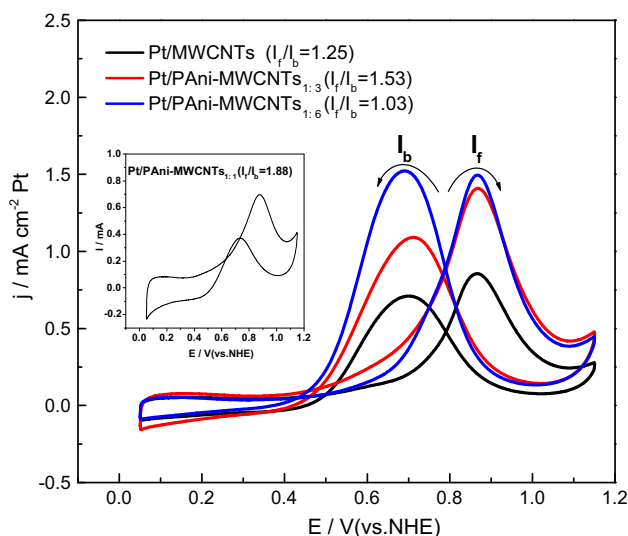


Fig. 6 Electro-catalytic properties of as-prepared catalysts in 0.5 M CH_3OH and 0.5 M H_2SO_4 . The scan rate is set at 50 mV s^{-1} (Embedded graph represents CV of Pt/PAni-MWCNT_{1:1}, but the current was not normalized by EASA)

1563 and 1476 cm^{-1} were due to C=C stretching vibration on quinoid and benzenoid rings, respectively. The bands at 1303 and 1228 cm^{-1} were assigned to the C–N stretching vibration on benzenoid ring. The band at 1123 cm^{-1} was attributed to in-plane bending vibration of C–H, which was introduced during protonation [18, 19]. PANi was therefore speculated to be in its highly conductive emeraldine state, as deduced from its FTIR spectrum. Similarities were observed in the spectrum of PANi-MWCNT_{1:1}, although with the shift of some bands. However, the characteristic absorption of MWCNT becomes predominant at a high MWCNT content.

Bright-field TEM images of PANi-MWCNT_{1:1}, PANi-MWCNT_{1:3} and PANi-MWCNT_{1:6} and MWCNT were shown in Fig. 2. The wall and cavity of MWCNT became less visible in PANi-MWCNT composites with the increase of loading level of PANi. Combining FTIR spectra and bright-field TEM images, it can be inferred that PANi-MWCNT composites with the different loading levels of PANi can be obtained upon different feed molar ratios between aniline and MWCNT.

Morphology of Pt/PAni-MWCNT catalysts

Bright-field TEM images of Pt/PAni-MWCNT catalysts were shown in Fig. 3 with calculated Pt particle size distribution plots attached as insets. In Fig. 3, Pt particles could be readily discerned as dark spots due to significantly higher electron density compared with PANi-MWCNT. And Pt particles supported by PANi-MWCNT composites possessed smaller sizes and narrower size distributions than

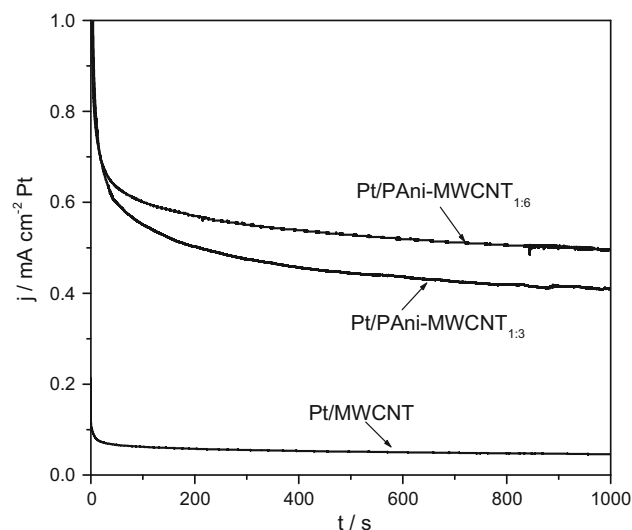


Fig. 7 Current–time curves in 0.5 M CH_3OH and 0.5 M H_2SO_4 solution at a fixed potential of 0.75 V (vs. NHE)

Pt particles barely supported by MWCNT. Obviously, the presence of PANi significantly improved the dispersion of Pt catalysts, and the loading level of PANi had also influence on the size distribution of Pt particles. The improved dispersion of Pt catalysts could be explained by lowered nucleation barrier where nitrogen was located in PANi via Pt–N bonding and large nucleation density for Pt crystal growth [20, 21].

XRD patterns of Pt/PAni-MWCNT catalysts

XRD patterns of Pt/MWCNT, Pt/PAni-MWCNT_{1:1}, Pt/PAni-MWCNT_{1:3} and Pt/PAni-MWCNT_{1:6} catalysts were shown in Fig. 4. Characteristic diffraction of MWCNT at $2\theta = 25.9^\circ$ was observed on all the samples. The other four strong diffraction peaks could be indexed to (111), (200), (220), and (311) planes of Pt crystal, respectively, indicating face-centered cubic (FCC) structure of Pt catalysts irrespective of the MWCNT or PANi-MWCNT supports [20, 22]. The average sizes of four catalysts can be calculated via the Debye–Scherrer formula:

$$d = \frac{0.89\lambda K\alpha_1}{B_{2\theta} \cos \theta_{\max}}$$

Where d is the mean dimension of crystalline particles, $\lambda_{K\alpha}$ is the wavelength of X-ray source, θ_{\max} is the angle of diffraction from (220) plane of Pt crystals, and $B_{2\theta}$ is the full width at half-maximum (FWHM) for Pt (220) diffraction peak. The estimated average size of Pt particles on Pt/PAni-MWCNT_{1:1}, Pt/PAni-MWCNT_{1:3}, Pt/PAni-MWCNT_{1:6} and Pt/MWCNT catalysts was 3.6, 3.5, 3.4 and 5.6 nm respectively, which further supported the morphological observation in bright-field TEM images. The finer

particle dispersion could improve the catalytic performance from increased specific surface area [5].

Electro-catalytic performance for methanol oxidation

In many electro-catalytic studies on methanol oxidation, the current densities can be normalized by the electrochemical active surface area (EASA) of Pt catalysts. And hydrogen adsorption/desorption peaks are usually used to evaluate EASA of Pt catalysts. Therefore, CVs of the as-

Table 1 Composition (at.%) of as-prepared catalysts resulting from XPS

Catalysts	C	O	N	Pt
Pt/MWCNT	86.88	11.79	/	1.33
Pt/PAni-MWCNT _{1:6}	87.35	9.64	1.35	2.08
Pt/PAni-MWCNT _{1:3}	82.68	13.4	2.27	1.66
Pt/PAni-MWCNT _{1:1}	83.02	10.15	4.75	1.66

prepared catalysts were recorded with 0.5 M H₂SO₄ at scan rate of 50 mV s⁻¹.

As shown in Fig. 5, in the potential region from 0.05 to 0.4 V (vs. NHE), characteristic hydrogen adsorption/desorption signals from (110) and (100) planes of polycrystalline Pt were observed on Pt/MWCNT, Pt/PAni-MWCNT_{1:3} and Pt/PAni-MWCNT_{1:6} catalysts [23], while they differed dramatically from Pt/PAni-MWCNT_{1:1} catalyst. In the above potential range, the electrochemical reduction of PAni could be expected and generate additional effect on the adsorption/desorption process at a high loading level of PAni. Therefore, EASA of Pt catalysts for the PAni-MWCNT_{1:1} can not be exactly evaluated by hydrogen adsorption/desorption peaks. The EASA is estimated from the equation:

$$\text{EASA} = Q_H / 0.21,$$

where “ Q_H ” is the electrical charge of hydrogen adsorption integrated from the CV curves, assuming monolayer hydrogen atom coverage and the hydrogen adsorption electrical charge being 0.21 mC cm⁻² smooth Pt surface

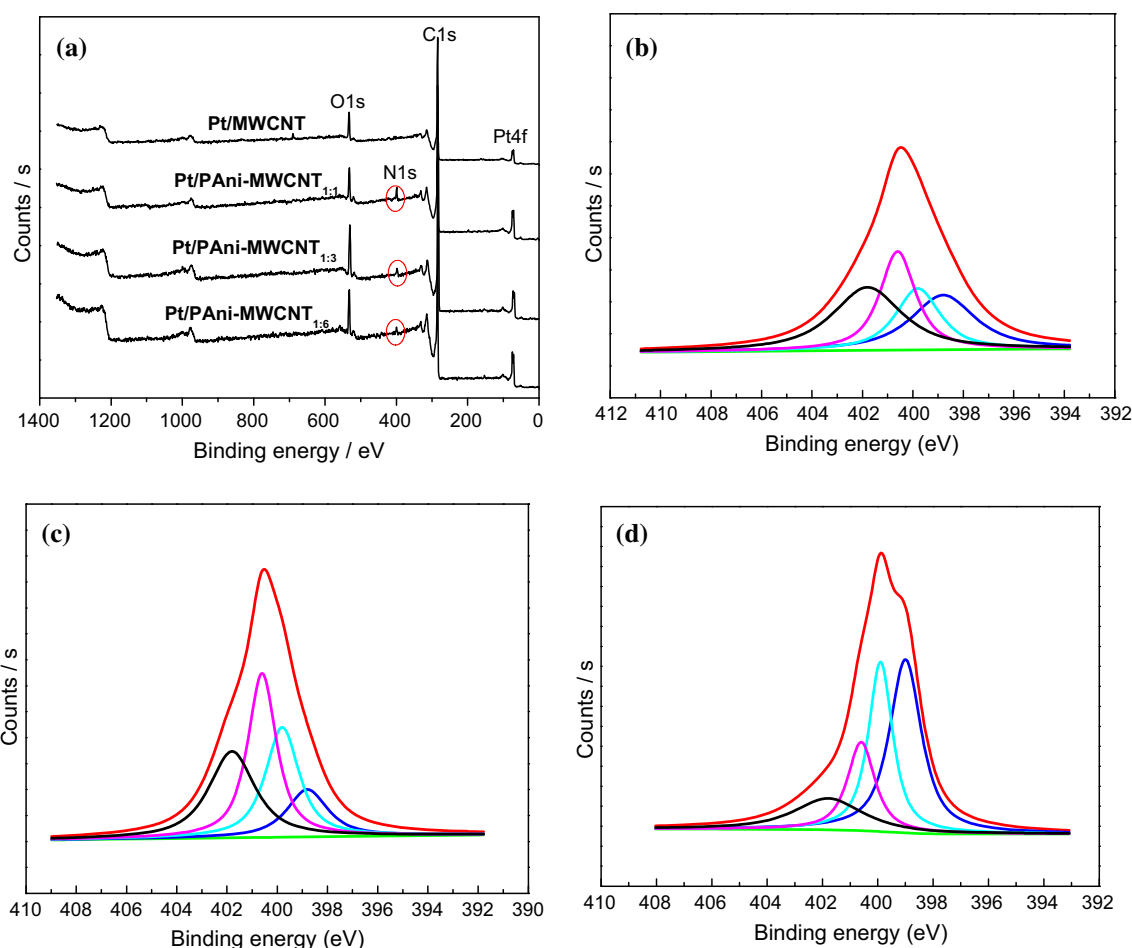


Fig. 8 XPS of Pt/MWCNT and Pt/PAni-MWCNT (a), N (1s) XPS of Pt/PAni-MWCNT_{1:6} (b), Pt/PAni-MWCNT_{1:3} (c), and Pt/PAni-MWCNT_{1:1} (d)

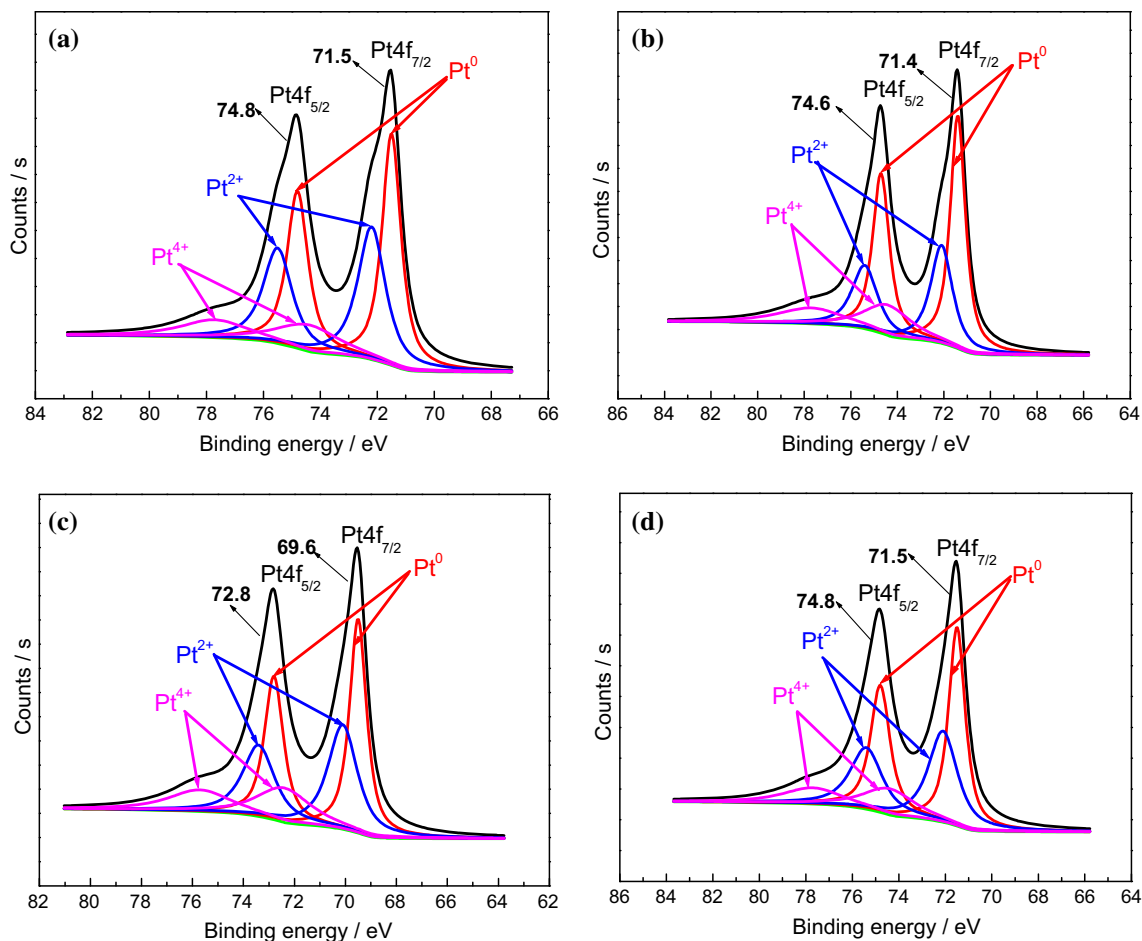


Fig. 9 Pt4f XPS of Pt/MWCNT (a), Pt/PAni-MWCNT_{1:6} (b), Pt/PAni-MWCNT_{1:3} (c), and Pt/PAni-MWCNT_{1:1} (d)

Table 2 The atomic ratio (at.%) of Pt(0)/Pt(II)/Pt(IV) of as-prepared catalysts

Catalysts	Pt(0) %	Pt(II) %	Pt(IV) %
Pt/MWCNT	46	38	16
Pt/PAni-MWCNT _{1:6}	50	30	20
Pt/PAni-MWCNT _{1:3}	43	36	21
Pt/PAni-MWCNT _{1:1}	40	38	22

[24]. The electrochemical active specific surface areas of Pt/MWCNT, Pt/PAni-MWCNT_{1:3} and Pt/PAni-MWCNT_{1:6} were calculated to be 233, 283, and 394 m² g⁻¹ Pt, respectively. Clearly, Pt/PAni-MWCNT_{1:6} showed a higher electrochemical active specific surface area than Pt/MWCNT and Pt/PAni-MWCNT_{1:3}, which may be related to the small size and good distribution of Pt catalyst.

Electro-catalytic properties of Pt/PAni-MWCNT_{1:3} and Pt/PAni-MWCNT_{1:6} catalysts for methanol oxidation were measured in 0.5 M CH₃OH and 0.5 M H₂SO₄, with Pt/MWCNT as control, as shown in Fig. 6. It is generally assumed that the two anodic peaks exhibit during methanol

oxidation correspond to two different states of Pt surface. Thus, it is widely accepted that Pt oxidation occurs during the anodic scan, followed by methanol oxidation that takes place on the oxidized surface, within the range of peak *I_f*. On the reverse cathodic scan, first, the reduction of platinum oxide begins, and then, methanol oxidation can occur on a clean, more or less oxide-free surface, at a lower potential (within the range of peak *I_b*) [25]. This explanation is also supported by the observation that the peak potential of *I_b* (from Fig. 6) matches well with that of the cathodic peak corresponding to Pt oxides reduction (from Fig. 5).

Methanol could be oxidized on the Pt/PAni-MWCNT_{1:6} and Pt/PAni-MWCNT_{1:3} catalysts at a lower potential compared to that on the Pt/MWCNT, and the current densities were also significantly higher, as evidenced by CV curves in Fig. 6. This could be interpreted by the improved efficiency of Pt catalysts [20].

To further study the activity and stability of Pt/PAni-MWCNT_{1:6} and Pt/PAni-MWCNT_{1:3} catalysts, CA measurements were performed at 0.75 V (vs. NHE) in 0.5 M CH₃OH and 0.5 M H₂SO₄ solution. Current–time curves

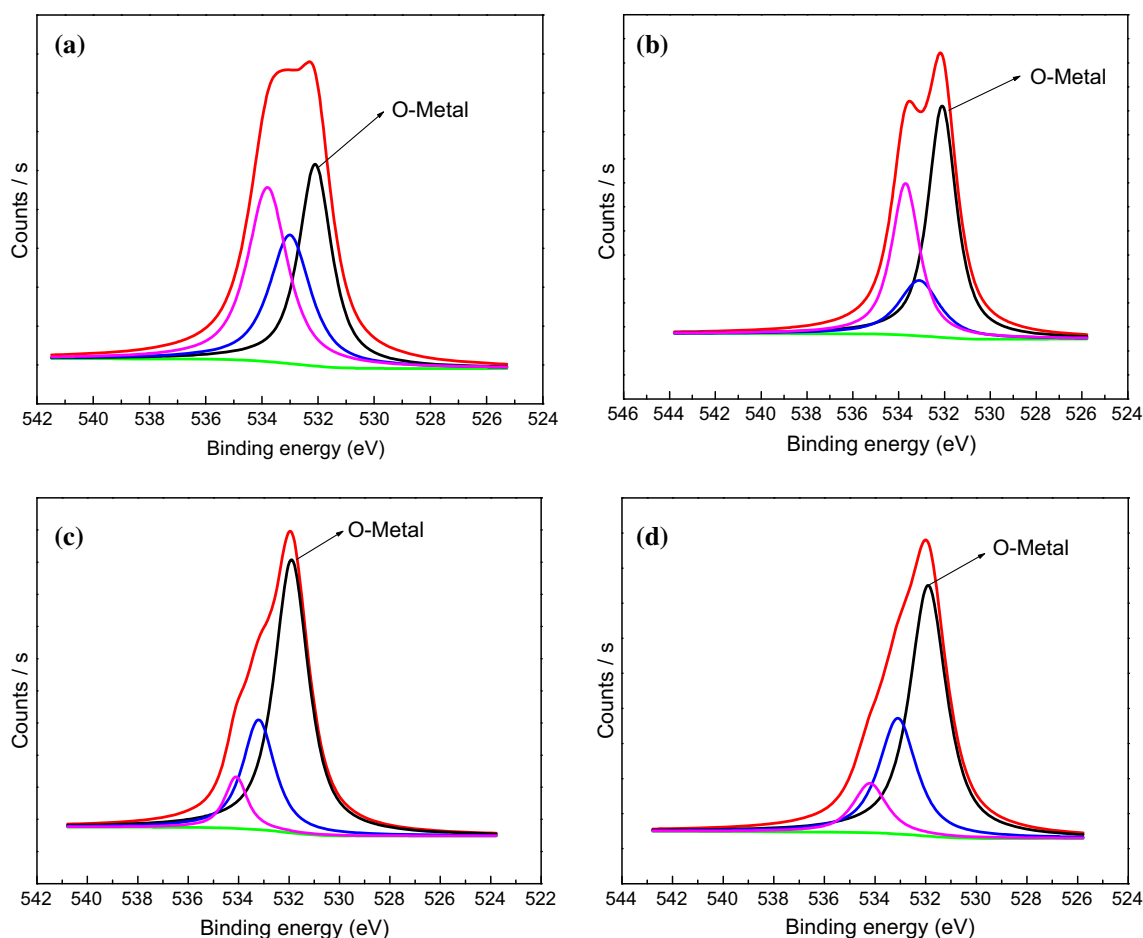


Fig. 10 O 1s XPS of Pt/MWCNT (a), Pt/PAni-MWCNT_{1:6} (b), Pt/PAni-MWCNT_{1:3} (c), and Pt/PAni-MWCNT_{1:1} (d)

Table 3 The proportion (%) of the various oxygen species resulting from O 1s spectra

Catalysts	~531.9 eV (O-metal)	~533.1 eV (C=O)	~534.2 eV (C–O)
Pt/MWCNT	43	18	39
Pt/PAni-MWCNT _{1:6}	54	12	34
Pt/PAni-MWCNT _{1:3}	72	19	9
Pt/PAni-MWCNT _{1:1}	61	29	10

were plotted in Fig. 7. Followed by a rapid decrease, the high initial currents of Pt/PAni-MWCNT_{1:3} and Pt/PAni-MWCNT_{1:6} were primarily ascribed to the double layer charging [26, 27]. After 1000 s, methanol electro-oxidation on Pt/PAni-MWCNT_{1:6} still possessed the highest limiting current density, indicating its superior catalytic activity and stability to others. These results clearly indicated that the loading level of PANi had an important impact on Pt catalyst size, size distribution, and catalytic activities for methanol oxidation.

XPS of as-prepared catalysts

XPS is one of the most powerful techniques that quantitatively probe the elemental compositions and the origin of chemical bonds on surface in the outermost region with thickness of 5–10 nm. The elemental compositions can be identified from the characteristic BEs of the photoelectrons and the peak intensity is proportional to the atomic concentration of elements [28]. The peak intensity is integrated from XPS intensity–BE curves. According to the loading level of PANi from TEM, it should be inferred that XPS could be an alternative to determine the elemental compositions of as-prepared catalysts. On the basis of XPS results, the elemental compositions for as-prepared catalysts were calculated and tabulated in Table 1. Within the probing area of XPS, the molar ratios of aniline and carbon in MWCNT were about 1:1.5, 1:4, and 1:8 in Pt/PAni-MWCNT_{1:1}, Pt/PAni-MWCNT_{1:3}, and Pt/PAni-MWCNT_{1:6} catalysts, respectively. This means that loading level of PANi increases with increasing the feed ratio of aniline, as already been evidenced qualitatively by FTIR

and TEM.

The XPS survey spectra of Pt/MWCNT and Pt/PAni-MWCNT were presented in Fig. 8a. In addition to C 1s and O 1s signals, Pt 4f signals were observed in all as-prepared catalysts. N 1s signals were only identified in Pt/PAni-MWCNT catalysts. As shown in Fig. 8b–d, the high-resolution spectrum of N 1s could be fitted with four components with BEs of 398.8, 399.8, 400.6 and 401.8 eV, corresponding to quinonoid imine (=N–), benzenoid amine (–NH–), protonated amine (–N⁺) and protonated imine (=N⁺), respectively [29]. The quinonoid imine (=N–) signal with BE of 398.8 eV was a solid evidence proving the presence of Pt–N bond [6], which facilitated the methanol electro-oxidation by reducing electron density on Pt [30, 31].

The high-resolution spectra of Pt 4f of as-prepared catalysts were shown in Fig. 9. Three valences of Pt could be identified and further analyzed based on doublet binding energy of Pt 4f_{7/2} and Pt 4f_{5/2} [6, 32]. Two pairs of peaks from the spin–orbital splitting of the 4f_{7/2} and 4f_{5/2} regions were due to Pt(II) valence state and Pt(IV) valence state. The atomic compositions of varied Pt species were calculated based on Pt4f spectra of as-prepared catalysts, as shown in Table 2. Half of Pt was in elementary state in Pt/PAni-MWCNT_{1:6}, indicating that the reduction of ionic Pt was far from being complete. As deduced from Table 2 and Fig. 6, the ratio (I_f/I_b) of the forward anodic peak current (I_f) versus the backward anodic peak current (I_b) decreased with increasing Pt(0)/Pt(II) atomic ratio. This was further proof that the anodic peak on the reverse scan was due to methanol oxidation on oxide-free platinum. As the Pt(0) increased, more methanol was oxidized on the reverse scan, resulting in the increase of I_b and consequently in a decrease of I_f/I_b . From Table 2, it appeared that the lowest Pt(0)/Pt(II) ratio was found for Pt/PAni-MWCNT_{1:1}, however, the corresponding I_f/I_b (1.88) ratio was the highest among as-prepared catalysts. EASA of Pt/PAni-MWCNT_{1:1} failed to be estimated, but the ratio I_f/I_b was obviously not affected by the normalization of the current. Pt(II) could be easily transformed to Pt–(OH)_{ads} via Pt–O_{ads} and Pt–O intermediates, and Pt–(OH)_{ads} was considered as the sole intermediate in the oxidation of Pt–(CO)_{ad} to CO₂. Therefore, the detailed studies on Pt(0)/Pt(II) ratio may direct design toward more efficient Pt catalysts. Moreover, Pt 4f on Pt/PAni-MWCNT_{1:3} in Fig. 9 also witnessed a shift to lower BE, indicating the presence of oxygen-containing ligands (OH[–], H₂O), which was beneficial to improve the catalytic performance for methanol electro-oxidation [33].

O 1s XPS of Pt/MWCNT and Pt/PAni-MWCNT catalysts were also presented in Fig. 10. Three components could be identified by curve fitting with the strongest one at BE of 531.5 eV, which may be interpreted as Pt–O_x bond,

such as Pt–O_{ads}, Pt–O and Pt–O₂. The atomic fractions of varied oxygen species were listed in Table 3. The largest O–Metal value was detected in Pt/PAni-MWCNT_{1:3}, which might also be beneficial to improve the tolerance of Pt-based catalysts [34].

Conclusions

For Pt/PAni-MWCNT catalysts, the loading level of PAni affected the proportion of the different valence Pt components. The proper proportion of Pt(II) was essential for coordination of Pt with oxygen-containing ligands (OH[–], H₂O) and thus accelerating oxidation of Pt (CO)_{ads} with release of CO₂ by improving the tolerance to intermediate carbonaceous species. In this study, a higher current density, better stability, and lower onset potential toward methanol oxidation were observed for Pt/MWCNT catalyst upon incorporation of conductive PAni, offering a new perspective on producing inexpensive high-performance DMFC catalyst at reduced Pt content.

References

- Sharma S, Pollet BG (2012) Support materials for PEMFC and DMFC electrocatalysts: a review. *J Power Sources* 208:96–119
- Veziroglu A, Macario R (2011) Fuel cell vehicles: state of the art with economic and environmental concerns. *Int J Hydrog Energy* 36:25–43
- Wang K, Hissel D, Péra MC, Steiner N, Marra D, Sorrentino M, Pianese C, Monteverde M, Cardone P, Saarinen J (2011) A review on solid oxide fuel cell models. *Int J Hydrog Energy* 36:7212–7228
- Gao H, He JB, Wang Y, Deng N (2012) Advantageous combination of solid carbon paste and a conducting polymer film as a support of platinum electrocatalyst for methanol fuel cell. *J Power Sources* 205:164–172
- Zhao HB, Li L, Yang J, Zhang YM (2008) Nanostructured polypyrrole/carbon composite as Pt catalyst support for fuel cell applications. *J Power Sources* 184:375–380
- He DP, Zeng C, Xu C, Cheng NC, Li HG, Mu SC, Pan M (2011) Polyaniline-functionalized carbon nanotube supported platinum catalysts. *Langmuir* 27:5582–5588
- Zhao X, Yin M, Ma L, Liang L, Liu CP, Liao JH, Lu TH, Xing W (2011) Recent advances in catalysts for direct methanol fuel cells. *Energy Environ Sci* 4:2736–2753
- Antolini E (2010) Composite materials: an emerging class of fuel cell catalyst supports. *Appl Catal B* 100:413–426
- Lota G, Fic K, Frackowiak EE (2011) Carbon nanotubes and their composites in electrochemical applications. *Energy Environ Sci* 4:1592–1605
- Tang SH, Sun GQ, Qi J, Sun SG, Guo JS, Xin Q, Haarberg GM (2010) Review of new carbon materials as catalyst supports in direct alcohol fuel cells. *Chin J Catal* 31:12–17
- Basri S, Kamarudin SK, Daud WRW, Yaakub Z (2010) Nanocatalyst for direct methanol fuel cell (DMFC). *Int J Hydrog Energy* 35:7957–7970
- Huang JE, Guo DJ, Yao YG, Li HL (2005) High dispersion and electrocatalytic properties of platinum nanoparticles on surface-

- oxidized single-walled carbon nanotubes. *J Electroanal Chem* 577:93–97
13. Liu Z, Lin X, Lee JY, Zhang W, Han M, Gan LM (2002) Preparation and characterization of platinum-based electrocatalysts on multiwalled carbon nanotubes for proton exchange membrane fuel cells. *Langmuir* 18:4054–4060
 14. MacDiarmid AG (2001) “Synthetic metals”: a novel role for organic polymers (nobel lecture). *Angew Chem Int Ed* 40: 2581–2590
 15. Wan MX (2009) Some issues related to polyaniline micro-/ nanostructures. *Macromol Rapid Commun* 30:963–975
 16. Antolini E, Gonzalez ER (2009) Polymer supports for low-temperature fuel cell catalysts. *Appl Catal A* 365:1–19
 17. Shao YY, Sui JH, Yin GP, Gao YZ (2008) Nitrogen-doped carbon nanostructures and their composites as catalytic materials for proton exchange membrane fuel cell. *Appl Catal B* 79:89–99
 18. Kang ET, Neoh KG, Tanh KL (1998) Polyaniline: a polymer with many interesting intrinsic redox states. *Prog Polym Sci* 23:277–324
 19. Rodrigues PC, Cantao MP, Janissek P, Scarpa PCN, Mathias AL, Ramos LP, Gomes MAB (2002) Polyaniline/lignin blends: FTIR, MEV and electrochemical characterization. *Eur Polym J* 38:2213–2217
 20. Zhang S, Wang H, Zhang N, Kong FD, Liu H, Yin GP (2012) Role of Pt-pyridinic nitrogen sites in methanol oxidation on Pt/polypyrrole–carbon black catalyst. *J Power Sources* 197:44–49
 21. Zhao YC, Zhan L, Tian JN, Nie SL, Ning Z (2011) Enhanced electrocatalytic oxidation of methanol on Pd/polypyrrole–graphene in alkaline medium. *Electrochim Acta* 56:1967–1972
 22. Zhang S, Shao YY, Yin GP, Lin YH (2009) Stabilization of platinum nanoparticle electrocatalysts for oxygen reduction using poly(diallyldimethylammonium chloride). *J Mater Chem* 19: 7995–8001
 23. Li YJ, Gao W, Ci LJ, Wang CM, Ajayan PM (2010) Catalytic performance of Pt nanoparticles on reduced graphene oxide for methanol electro-oxidation. *Carbon* 48:1124–1130
 24. Huang T, Jiang RR, Liu JL, Zhuang JH, Cai WB, Yu AS (2009) Synthesis of well-dispersed PtRuSnOx by ultrasonic-assisted chemical reduction and its property for methanol electrooxidation. *Electrochim Acta* 54:4436–4440
 25. Delahay P (1965) Double layer and electrode kinetics. Wiley, New York
 26. Tsiouvaras N, Martínez-Huerta MV, Moliner R, Lázaro MJ, Rodríguez JL, Pastor E, Peña MA, Fierro JLG (2009) CO tolerant PtRu–MoOx nanoparticles supported on carbon nanofibers for direct methanol fuel cells. *J Power Sources* 186:299–304
 27. Wang ZB, Yin GP, Zhang J, Sun YC, Shi PF (2006) Co-catalytic effect of Ni in the methanol electro-oxidation on Pt–Ru/C catalyst for direct methanol fuel cell. *Electrochim Acta* 51:5691–5697
 28. Golczak S, Kanciurowska A, Fahlman M, Langer K, Langer JJ (2008) Comparative XPS surface study of polyaniline. *Thin Films Solid State Ionics* 179:2234–2239
 29. Kang ET, Neoh KG, Tan KL (1993) X-ray photoelectron spectroscopic studies of electroactive polymers. Springer, Berlin Heidelberg 106:135–190
 30. Maiyalagan T, Viswanathan B (2005) Nitrogen containing carbon nanotubes as supports for Pt- alternate anodes for fuel cell applications. *Electrochem Commun* 7:905–912
 31. Roy SC, Harding AW, Russell AE, Thomas KM (1997) Spectroelectrochemical study of the role played by carbon functionality in fuel cell electrodes. *J Electrochem Soc* 144:2323–2328
 32. Parkinson CR, Walker M, McConville CF (2003) Reaction of atomic oxygen with a Pt (111) surface: chemical and structural determination using XPS, CAICISS and LEED. *Surf Sci* 545:19–33
 33. Drelinkiewicz A, Zieba A, Sobczak JW, Bonarowska M, Karpin’ski Z, Waksmundzka-Góra A, Stejskal J (2009) Polyaniline stabilized highly dispersed Pt nanoparticles: preparation characterization and catalytic properties. *React Funct Polym* 69:630–642
 34. Li G, Picku PG (2007) Decoration of carbon-supported Pt catalysts with Sn to promote electro-oxidation of ethanol. *J Power Sources* 173:121–129